Light-induced nonthermal population of optical phonons in nanocrystals

Bruno P. Falcão,[1,*] Joaquim P. Leitão,[1] Maria R. Correia,[1] Maria R. Soares,[2]
Hartmut Wiggers,[3] Andrés Cantarero,[4] and Rui N. Pereira[1,5]

[1]*Departamento de Física and I3N, Universidade de Aveiro, Campus Universitário de Santiago, 3810-193 Aveiro, Portugal*
[2]*Laboratório Central de Análises, Universidade de Aveiro, Campus Universitário de Santiago, 3810-193 Aveiro, Portugal*
[3]*Institut für Verbrennung und Gasdynamik and CENIDE, Universität Duisburg-Essen, 47057 Duisburg, Germany*
[4]*Instituto de Ciencia Molecular, Universidad de Valencia, E-46071 Valencia, Spain*
[5]*Walter Schottky Institut and Physik-Department, Technische Universität München, Am Coulombwall 4, 85748 Garching, Germany*

(Received 30 December 2016; revised manuscript received 7 March 2017; published 30 March 2017)

Raman spectroscopy is widely used to study bulk and nanomaterials, where information is frequently obtained from spectral line positions and intensities. In this study, we monitored the Raman spectrum of ensembles of semiconductor nanocrystals (NCs) as a function of optical excitation intensity (*optical excitation experiments*). We observe that in NCs the red-shift of the Raman peak position with increasing light power density is much steeper than that recorded for the corresponding bulk material. The increase in optical excitation intensity results also in an increasingly higher temperature of the NCs as obtained with Raman thermometry through the commonly used Stokes/anti-Stokes intensity ratio. More significantly, the obtained dependence of the Raman peak position on temperature in optical excitation experiments is markedly different from that observed when the same NCs are excited only thermally (*thermal excitation experiments*). This difference is not observed for the control bulk material. The inefficient diffusion of photogenerated charges in nanoparticulate systems, due to their inherently low electrical conductivity, results in a higher steady-state density of photoexcited charges and, consequently, also in a stronger excitation of optical phonons that cannot decay quickly enough into acoustic phonons. This results in a nonthermal population of optical phonons and thus the Raman spectrum deviates from that expected for the temperature of the system. Our study has major consequences to the general application of Raman spectroscopy to nanomaterials.

DOI: 10.1103/PhysRevB.95.115439

I. INTRODUCTION

Raman spectroscopy (RS) is a nondestructive, simple, and highly sensitive technique that has been widely used to study different materials in various forms and dimensions by means of their characteristic vibrational signatures. The versatility and instrumental development of RS have made it one of the most popular characterization techniques in the fields of geology [1], biology [2], semiconductor materials [3], and polymer science [4], both at academic and industrial levels. In the field of semiconductors, a large variety of bulk crystalline materials has been investigated by RS, including those of group IV [5–7], III-V materials [7–9], and III-nitrides [10–14]. RS has also been a valuable tool to investigate low-dimensional semiconductor structures, such as superlattices [15], nanowires [16–18], and nanocrystals [19,20], as well as more exotic nanomaterials such as graphene [21–23] and carbon nanotubes [24–26].

The Raman spectrum can provide detailed information about many physical properties, including structure, composition, strain, material size, electronic doping, and local temperature. For instance, temperature measurements using RS (Raman thermometry) can be carried out by analyzing variations in Raman spectra resulting from changes in zone-centered optical phonons, namely, changes in Stokes and/or anti-Stokes Raman peak position (Ω) and/or linewidth (Γ), or variations in the ratio between the peak intensities observed in the Stokes and anti-Stokes regions of the spectrum [6,27–31]. Also, strain-related effects, originating from crystal defects, lattice and/or thermal mismatches, can be unveiled by analyzing variations in Ω and/or Γ [32–34]. The nature and concentration of doping in a semiconductor can also be investigated through shifts observed in Ω and changes in Raman peak shape, which result from the so-called Fano interference between optical phonons and the electronic state continuum [32,35–38]. Moreover, shifts in Ω and broadening of Γ due to quantum confinement of phonons in low-dimensional structures have been exploited to estimate the size of nanocrystallites [39–46]. Hence, a single parameter of the Raman spectrum, for example the peak position Ω, can depend on several physical effects, namely, temperature, strain, doping, and quantum confinement, amongst others. Importantly, these effects can simultaneously influence the spectrum measured in one Raman experiment. For example, it is known that a Raman spectrum of quantum-confined nanocrystals heated to a certain temperature (e.g., by optical excitation during the Raman measurement) will experience a shift in Ω due to both quantum-confinement and temperature effects, whose deconvolution is not straightforward [43,45,47–49]. The situation becomes even more complicated if unexpected effects contribute to the Raman spectrum parameters. This is particularly relevant in the case of nanomaterials since their physical properties tend to differ from those known for their bulk counterparts. We expect this to be the case in silicon nanocrystals (Si-NCs) where it has been found that under high optical excitation intensity the dependence of the Raman peak position Ω, associated with the Raman active optical phonon mode, on temperature, as measured by means of Raman thermometry, is more abrupt than that observed for bulk crystalline silicon (c-Si) [43,46–48,50]. In general, RS

*bfalcao@ua.pt

can only provide reliable information if all factors contributing to the Raman parameter under analysis are known.

In this work, we conclude that for nanocrystals under moderate/strong optical pumping, the Raman peak position Ω is influenced by the inherently low electrical transport in nanomaterials. We study this phenomenon using free-standing Si-NCs by measuring the temperature and excitation power dependencies of the Raman scattering and comparing with those observed for bulk *c*-Si. The differences observed in the behavior of Raman spectra measured under optical and thermal excitation conditions are discussed in the scope of a different population of optical phonons associated to a stronger influence of the electron-phonon coupling, which results from a hindered diffusion of photoexcited charge carriers in nanoparticulate systems. We notice that silicon provides an unmatched platform for studying such kind of effects in nanomaterials due to its long technological history and the deep understanding of its Raman spectrum. Besides, there is an increasing interest in electronic and optoelectronic devices based on low-dimensional silicon structures, in particular Si-NCs. They offer an enormous range of tunability of their physical properties through size, shape, doping, and embedding material, which brings a huge potential for applications such as light sources [51–53], flash memories [54,55], and high efficient solar cells [56–58]. Not surprisingly, there have been an increasing number of publications concerning the investigation of the Si-NCs physical properties by RS [59–61], particularly the determination of the nanocrystals size and temperature from the Raman peak position Ω of the optical phonon [45–47,49].

II. EXPERIMENTAL DETAILS

Free-standing Si-NCs in the powder form and with a surface termination with Si-H bonds (H termination) were synthesized from gas phase in a silane (SiH_4) plasma [62]. After prolonged exposure of these Si-NCs to air, a thin ($\sim$1.5nm thick) silicon oxide shell is formed on the surface [63]. Several samples with different mean crystallite sizes were produced and studied. The mean crystallite sizes were estimated by carrying out a Williamson-Hall profile analysis of X-ray diffraction (XRD) patterns obtained in experiments performed in the Bragg-Brentano geometry with a PANalytical X'Pert MPD diffractometer using Cu-K_α radiation. XRD data are shown in the Supplemental Material [64]. For the sake of simplicity, we label the different samples used in this study according to their mean crystallite diameter determined from XRD. Samples for Raman measurements consisted of Si-NCs deposited onto borosilicate glass substrates (ProSciTech Pty Ltd). The Si-NCs deposition was carried out by spin coating of dispersions containing Si-NCs dispersed in absolute ethanol (3 wt.%). The dispersion was achieved by combining several sonication and stirring processes. The resulting NC samples consist of multilayer films with thickness up to 2 μm (see Supplemental Material [64]), with a density around 30%–40% [19]. Raman scattering measurements were performed in backscattering configuration in a Jobin-Yvon LabRam HR 800 spectrometer equipped with a Peltier-cooled (203 K) CCD detector and an ULF filter pack for Stokes and anti-Stokes analysis. All measurements were carried out with a 50$\times$ long focal distance objective (0.5 numerical aperture), which resulted in a probing spot radius of $\sim$0.7 μm. The Raman measurements were done with either the 532-nm or 633-nm line of diode pumped solid state (Laser Quantum) and He-Ne (CVI Melles Griot) lasers, respectively. In the *optical excitation experiments*, the samples were measured without external heating with laser power densities that varied in the range 10^3–10^6 W/cm^2 using neutral density filters. In the *thermal excitation experiments*, the samples were placed on a Linkam THMS600 temperature controlled stage that allowed control of their temperature in the range from room temperature to 873 K. Here, the laser power was kept low to avoid light-induced heating of the samples. The samples were kept under vacuum conditions ($<10^{-2}$ mbar) during all Raman measurements. Control and comparative Raman measurements were also carried out for bulk *c*-Si using a piece of an intrinsic silicon wafer, which also enabled calibration of the Raman spectrometer.

III. RESULTS AND DISCUSSION

Figure 1 shows representative Raman spectra obtained at room temperature for Si-NCs with different mean diameter and measured using different laser wavelengths [spectra Figs. 1(b)–1(e)]. All spectra were probed with excitation power densities above 190 kW/cm^2. For comparison purposes, characteristic spectra from bulk *c*-Si, showing the typical optical phonon mode peak at $\Omega = 521.5$ cm^{-1}, and from hydrogenated amorphous Si (*a*-Si:H), with the usual broad asymmetric band with maximum at $\sim$480 cm^{-1}, are also shown [spectra Figs. 1(a) and 1(f), respectively]. As can be seen, the spectra of Si-NCs show peaks that are deviated towards lower frequencies (red-shifted) when compared to the peak observed for bulk *c*-Si, when similar excitation powers are used. A larger frequency red-shift of the peaks in the Si-NCs spectra is accompanied by an increased line broadening. The shapes of the peaks observed for the Si-NCs are nicely fitted with Lorentzian curves, similar to the case of the bulk *c*-Si Raman peak [see Fig. 1(a)]. From the fits, we found that the peaks observed for Si-NCs exhibit red-shifts as high as 30 cm^{-1}. This results in the appearance of peaks with Ω close to the frequency of the band typically observed for *a*-Si:H [see Fig. 1(f)]. However, these peaks cannot originate from an amorphous silicon phase in our samples because their shape and width are completely different from those observed for *a*-Si:H, whose Raman band is commonly described by the sum of two Gaussian curves [65]. Besides, the XRD analysis show only the presence of crystalline silicon (see Supplemental Material [64]). Raman peaks strongly deviated toward low energies are observed in measurements carried out with both excitation wavelengths λ_{exc} of 532 and 633 nm [see, for example, spectra Figs. 1(d) and 1(e)], which correspond both to strongly absorbing photons (above energy band gap). We have found that the number of peaks observed in the Raman spectra does not show any coherent dependence on the excitation wavelength or sample (nanocrystallite size). For the same sample (Si-NC film), we found a range of situations, i.e., spectra with one peak, spectra with two peaks, and spectra with more than two peaks. Instead, we find that the number of peaks depends on the particular measurement spot within the sample. For simplicity, in Figs. 1(b)–1(e) we show only

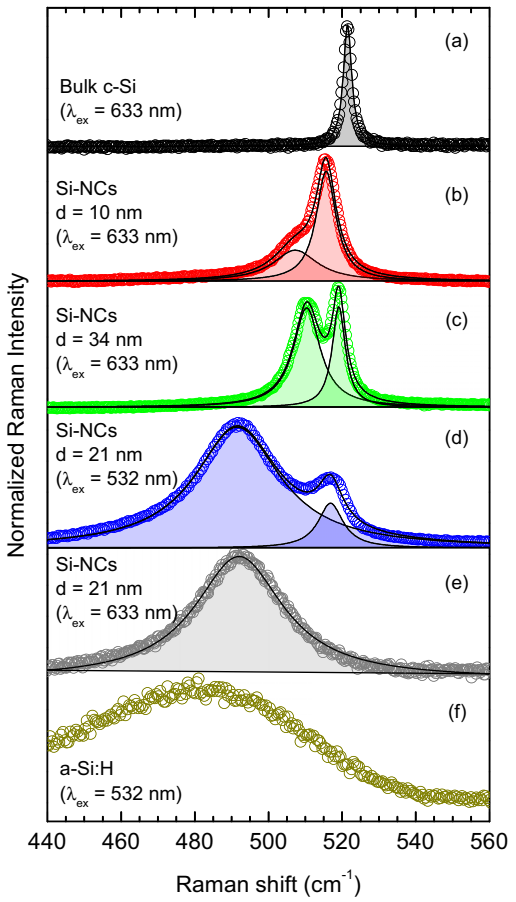

FIG. 1. Raman spectra of (b)–(e) different Si-NCs samples, with various crystallite sizes, in comparison with the (a) bulk c-Si and (f) amorphous Si spectra. The Raman spectrum of bulk c-Si features a single peak related to the zone-center optical phonon mode, whereas the one of amorphous phase is characterized by a broad asymmetric band at lower frequencies. The Si-NCs spectra may evidence one or more peaks, irrespectively of the nanocrystallite size (d) and excitation wavelength (λ_{exc}). The solid lines represent fits to the spectra using Lorentzian curves.

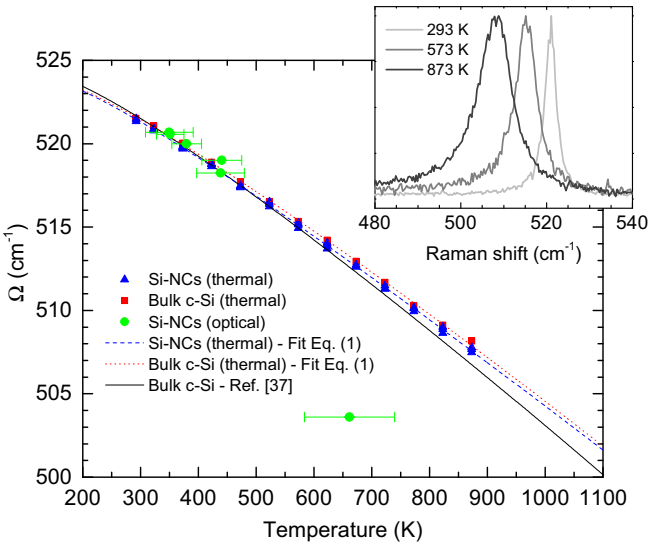

FIG. 2. Temperature dependence of the frequency of the optical phonon mode observed in *thermal excitation experiments* of a Si-NCs (34 nm) film and of bulk c-Si. The inset shows representative Raman spectra from the same Si-NCs film at different temperatures. The parameters used to calculate the solid, dashed, and dotted lines are listed in Table I.

spectra containing up to two peaks since in cases containing more peaks the deconvolution of the spectra is unreliable. We will return to this point below in the discussion.

Strongly red-shifted and broadened peaks have been observed recently by several authors in Raman spectra of Si-NCs [43,45–50,66–68]. In the cases where the Si-NCs are significantly large, so that phonon confinement effects could be ruled out, red-shifts up to 30 cm^{-1} and linewidths up to 22 cm^{-1} were observed [49,66], which are in line with those reported here. In general, these observations were explained exclusively based on a temperature increase of the NCs due to the optical excitation underlying the Raman experiment [43,45–50,66–68]. To investigate this phenomenon in more detail, we have carried out a comparative study of the effect of the temperature T and of the optical excitation intensity on the Raman spectra of Si-NCs and bulk c-Si. Thus, we first thoroughly study the temperature dependence of the Raman spectra of Si-NCs and compare it with the data obtained when we carry out similar experiments with bulk c-Si (*thermal excitation experiments*). In addition, we compare our experimental data with data reported in the literature for bulk c-Si.

In the thermal excitation experiments, in order to avoid local heating induced by the laser light, the excitation power density was kept at the lowest value while enabling the observation of both Stokes and anti-Stokes spectra. The excitation powers used for Si-NCs (5 kW/cm^2) and bulk c-Si (64 kW/cm^2) were maintained constant. In the case of Si-NCs, for each temperature T we have probed the sample at three different locations to assure representative data. The Raman spectra of the Si-NCs feature just a single peak, as shown for three different temperatures in the inset of Fig. 2. The spectra at each temperature were fitted with a single Lorentzian curve, from which the parameter Ω was extracted. These data are shown as a function of T in Fig. 2 (blue triangles). As can be seen, Ω progressively shifts towards lower frequencies with the increase of temperature. This trend follows closely the behavior observed when we perform similar temperature-dependent experiments with bulk c-Si (see Fig. 2, red closed squares) over the entire temperature range (293–873 K).

The temperature dependence of Ω results from the anharmonic coupling between the involved phonon and other phonons (phonon-phonon interactions) as well as on the thermal expansion of the crystal [6,27,70]. In the simplest case, the variation of the Raman line position with temperature can be expressed as [37]

$$\Omega(T) = \omega_0 + \Delta_{anh}(T) + \Delta_{latt}(T), \quad (1)$$

where ω_0 is the frequency observed at 0 K. $\Delta_{anh}(T)$ represents the anharmonic terms in the lattice potential, and $\Delta_{latt}(T)$ describes the thermal expansion. The anharmonic part of $\Omega(T)$

TABLE I. Values of the parameters obtained in the fitting of Eq. (1) to the data of the temperature dependence of Ω of the optical phonon mode for the Si-NCs and bulk *c*-Si, obtained in the thermal excitation experiments. Published values for bulk *c*-Si are also listed. For all cases, the term describing the thermal expansion of the lattice has been parametrized using values from Refs. [6,69].

Sample		ω_0 (cm^{-1})	C (cm^{-1})	D (cm^{-1})	F
Si-NCs	This work	527.6 ± 0.2	-3.4 ± 0.2	-0.02 ± 0.02	0.65 ± 0.08
Bulk *c*-Si	This work	527.3 ± 0.3	-3.1 ± 0.2	-0.04 ± 0.02	0.81 ± 0.03
	Ref. [37]	528	-3.45	-0.05	

has been described as [27]

$$\Delta_{\text{anh}}(T) = C\left(1 + \frac{2}{e^x - 1}\right) + D\left(1 + \frac{3}{e^y - 1} + \frac{3}{(e^y - 1)^2}\right), \tag{2}$$

where $x = \hbar\omega_0/2k_BT$, $y = \hbar\omega_0/3k_BT$, in which $\hbar$ is the reduced Planck constant and k_B is the Boltzmann constant; C and D are the so-called anharmonic parameters. The contribution of thermal expansion to the frequency shift can be described in the Grüneisen approximation as [6,70]

$$\Delta_{\text{latt}}(T) = \omega_0\left[\exp\left(-3\gamma\int_0^T \alpha(T)dT\right) - 1\right]. \tag{3}$$

Here, γ is the (isothermal) Grüneisen parameter and $\alpha(T)$ is the temperature dependence of the linear thermal expansion coefficient [69].

The dashed (dotted) lines in Fig. 2 illustrate the fits described with Eq. (1) to the temperature dependence of Ω obtained in our experiments for the Si-NCs (bulk *c*-Si). The corresponding fitting parameters obtained are listed in Table I. The solid line in Fig. 2 represents the well-known temperature dependence reported for bulk *c*-Si [37]. As can be seen in Table I, the obtained values for Si-NCs and bulk *c*-Si are very close to each other and are also close to the values reported in the literature for bulk *c*-Si. This observation reflects the close agreement between the temperature dependencies measured in our experiments for Si-NCs and bulk *c*-Si and the dependence reported for bulk *c*-Si [37]. In addition, it also shows that the temperature of the Si-NCs (and bulk *c*-Si) is very close to the experimental nominal temperature, which corresponds to the temperature of our sample holder.

Figure 3 shows the dependence of the Raman spectra of Si-NCs and bulk *c*-Si on the optical excitation intensity (*optical excitation experiments*). For Si-NCs probed under the lowest power density (5 kW/cm^2), the spectrum features a single peak at ∼521 cm^{-1} that progressively shifts towards lower frequencies and broadens with increasing the excitation power density. At the highest excitation power density (670 kW/cm^2), the spectrum displays a pair of peaks (centered at ∼504 and 518 cm^{-1}) instead of the single peak observed for the other power values. For bulk *c*-Si (dashed gray spectra), the Raman peak also red-shifts and broadens with the increase of the excitation power density but at much lower rate than that observed for Si-NCs. For both Si-NCs and bulk *c*-Si, the local temperature was evaluated by means of the commonly used procedure in Raman thermometry based on the ratio R between the intensities I_S and I_{AS} of the Stokes and anti-Stokes Raman bands, respectively, following the equation

$$R = \frac{I_S}{I_{AS}} = F\exp\left(\frac{\hbar\omega_0}{k_BT}\right), \tag{4}$$

where F is a coefficient that depends on the optical properties of the material and on measurement apparatus characteristics [71]. Detailed information regarding the determination of F is given in Supplemental Material [64]. It is found that the optical excitation promotes a much higher heating in the Si-NCs than in bulk *c*-Si, as observed in previous experiments from other authors [50,66,68,72]. In the samples, the Si-NCs form a very porous network with a rather poor inter-NC physical contact (grain boundary). This results in a very low thermal conductivity of the Si-NC samples when compared to bulk *c*-Si [45,46,49,61,68,73,74]. Therefore, the Si-NCs temperature increases due to optical excitation is much higher than when bulk *c*-Si is excited under the same conditions. In fact, due to the lack of signal intensity in the anti-Stokes region, the measurement of the Raman spectra of bulk *c*-Si

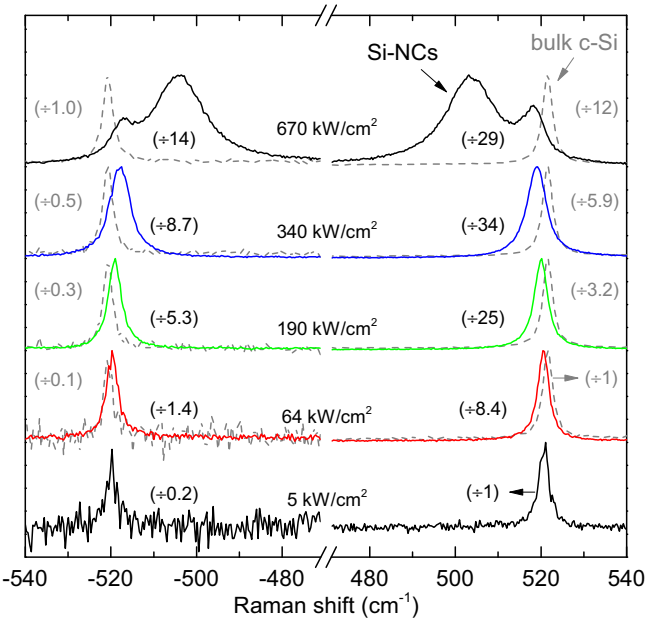

FIG. 3. Normalized anti-Stokes and Stokes Raman spectra measured at different excitation power densities ($\lambda_{exc} = 633$ nm) for one of the Si-NCs samples ($d = 34$ nm). The dashed lines represent the Raman spectra of bulk *c*-Si measured under the same conditions. The spectra were normalized to the Stokes spectrum measured with the lowest excitation power density; the normalization factors are shown between black and gray brackets for the Si-NCs and bulk *c*-Si, respectively.

was only achieved using an excitation power density one order of magnitude higher (64 kW/cm^2) than in the case of the Si-NCs. The intensity of anti-Stokes peaks increases with the raise of temperature. Another effect that may be contributing to the stronger Raman signals of Si-NCs is their lower optical reflectivity, resulting from an effective medium with lower refractive index, which enhances the rate of Raman scattering events.

The green circles in Fig. 2 show the variation of Ω as a function of temperature obtained from the excitation-power-dependent measurements illustrated in Fig. 3. As can be seen, for high optical excitation intensity, there is a clear deviation with respect to the expected Ω versus temperature dependence (blue triangles). This deviation is observed for the experimental point with lowest Ω and corresponding highest estimated temperature. In order to investigate this behavior more deeply, we have carried out experiments of the excitation power dependence of the Raman spectrum for different samples of the same Si-NCs ($d = 34$ nm) and also of different Si-NCs ($d = 10, 11, 21$ nm). The spectra have been evaluated following the same procedure as the one described above for the data in Fig. 3. The resulting values of Ω versus temperature are depicted in Fig. 4. Also plotted in this graph are the curves that describe the temperature behavior of Ω reported for bulk c-Si [37], and those determined in our thermal excitation experiments for the Si-NCs and bulk c-Si (from Fig. 2). In Fig. 4, we can see that the deviation between experimental data of Ω and the dependence expected for bulk c-Si is observed for all Si-NC samples studied. The experimental points observed in the higher range of Ω, i.e., $514 < \Omega < 521$ cm^{-1}, are close to the values expected for bulk c-Si. This closeness is more evident for Si-NCs with 34 nm, whereas for the other sizes, a small downshift of Ω values is observed. These deviations are most likely related to confinement effects resulting from the smaller size of these Si-NCs [39–42,44]. In the range of smaller Ω values ($\Omega < 514$ cm^{-1}), the deviations observed between the experimental data shown in Fig. 4 and the temperature dependence expected for bulk c-Si (solid and dotted lines) and also for Si-NCs (dashed line) cannot be explained based on confinement effects. Therefore, it becomes clear that the interaction of the excitation light with the Si-NCs promotes a frequency shift of the optical mode peak versus T, when T is obtained using Eq. (4), that is different from the shift obtained in the thermal excitation experiments. We will discuss the origin of this effect below.

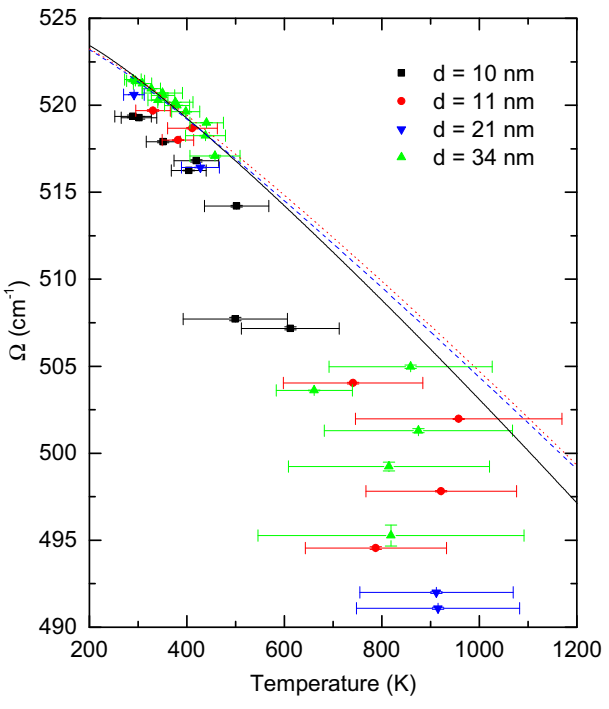

FIG. 4. Temperature dependence of the Raman peak position obtained in *optical excitation experiments* for different Si-NC samples (with the indicated crystallite sizes d). The solid, dashed, and dotted lines illustrate the $\Omega(T)$ dependencies reported for bulk c-Si, and those obtained in thermal excitation experiments for Si-NCs and bulk c-Si, respectively (see Table I).

When the Si-NCs are excited thermally (*thermal excitation experiments*), the vibrational state of the optical phonon mode with the highest population, denoted n, is only defined by the temperature T of the Si-NCs. In this case, the relation between n and T for the Si-NCs corresponds to that taking place for bulk c-Si, as demonstrated by the data shown in Fig. 2. Note that the frequency Ω of Raman line is directly determined by n and decreases with temperature due to anharmonicity. Similarly, the ratio f between the populations of the vibrational states $n + 1$ and n, denoted p_{n+1} and p_n, respectively, also depends only on the Si-NCs temperature and the relation f vs T is simply given by

$$f = \frac{p_{n+1}}{p_n} = \exp\left(\frac{\hbar\omega_0}{k_B T}\right). \quad (5)$$

Obviously, this is the reason why in Raman thermometry the temperature is frequently obtained from the ratio R between Stokes and anti-Stokes Raman lines using Eq. (4). Note that f is directly proportional to the ratio R given in Eq. (4). Hence, in our thermal excitation experiments with Si-NCs and bulk c-Si, n and f are only determined by the temperature of the system. Therefore, there is a well-defined relation between n (or Ω) and f (or R) when the temperature is changed. The relation between Ω and R obtained for Si-NCs from the data shown in Fig. 2, by solving Eq. (4) with respect to T and introducing the result in Eq. (1), is shown in Fig. 5 (dashed line). In the same figure are also plotted the experimental data obtained from our optical excitation experiments with Si-NCs (orange symbols). As can be seen, under optical excitation Ω vs R displays a clear deviation from the behavior expected if n (and f) is only determined by the temperature, which is the case in the thermal excitation experiments.

Upon optical pumping, the excitation of the optical phonon mode occurs in a way fundamentally different from that of the thermal excitation case. Under optical excitation with above energy band-gap photons, electrons (holes) are excited above (below) the conduction (valence) band edge. When these hot electrons and holes lose energy to occupy states in the corresponding band edges, they generate optical phonons (photocarrier thermalization) due to electron-phonon coupling. In turn, the optical phonons decay into acoustic phonons via phonon-phonon coupling, which results in generation of

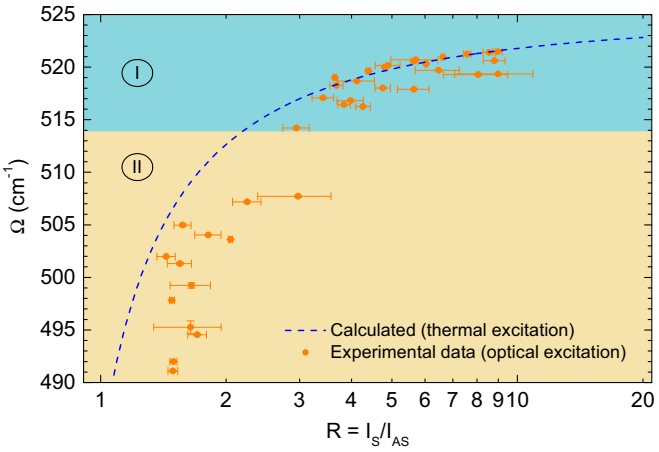

FIG. 5. Raman peak position Ω *versus* intensity ratio R. The dots (orange) represent the experimental data obtained for all Si-NC samples (data corresponding to Fig. 4). The dashed line (blue) depicts the expected (calculated) relationship between Ω and R (see text for details). The calculated dependence was obtained using the parameters shown in Table I, extracted from the thermal excitation experiments.

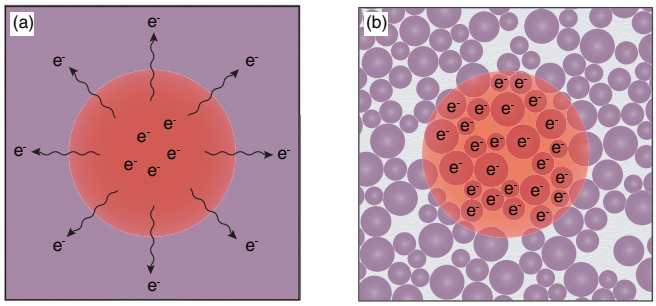

FIG. 6. Schemes representing the (a) allowed and (b) hindered diffusion of photoexcited electrons away from the Raman measurement (excitation) spot in a bulk material and in a nanoparticulate system, respectively. The red area represents the measurement (excitation) spot. In the nanoparticulate system, the higher steady-state density of photoexcited electrons in the measurement spot leads to an enhanced excitation of optical photons resulting from electron-photon coupling.

acoustic phonons and in sample heating. Thus, in the case of optical excitation, the state n of the optical phonon mode is determined by the balance between the energy gained from photogenerated carriers via electron-phonon interaction and the energy lost to acoustic phonons via phonon-phonon coupling. Likewise, the ratio f is also determined by the balance between these two energy terms.

Under low optical pumping conditions, the optical phonon generation rate is low and phonon-phonon coupling processes are sufficiently efficient so that the optical phonon population distribution, likewise n and f, corresponds to that expected for the temperature of the system. In this case, the system is in thermal equilibrium and Eq. (5) is applicable. Therefore, Ω vs R is close to that observed in a thermal excitation experiment (region I in Fig. 5). However, under moderate/high optical excitation intensity, the generation rate of optical phonons is higher. This generation rate may be so high that the optical phonons cannot decay into acoustic phonons quickly enough to bring the system to thermal equilibrium. There is no quick enough exchange of energy between optical and acoustic phonons and no thermal equilibrium is reached. Under these conditions, a nonthermal steady-state population of optical phonons is reached and, consequently, the populations p_n and p_{n+1} deviate from values expected for the temperature of the system. In other words, these populations can no longer be described by the Maxwell-Boltzmann statistics and, therefore, Eq. (5) is not valid anymore. The observed deviation of Ω vs R under intense optical excitation (region II in Fig. 5) is a direct evidence for a nonthermal optical phonon population distribution. This deviation occurs only in the case of the Si-NCs because of an enhanced effect of the electron-phonon coupling. More specifically, the rate of hot electron (hole) to optical phonon energy transfer events (optical phonon generation) is higher in the NCs than in the bulk, which leads to a higher optical phonon generation rate in the NCs.

We propose that this effect results from a hindered photocarrier diffusion in NCs due to their inherently low electrical conductivity. In the case of bulk c-Si, a considerable amount of photoexcited electrons lose their energy, during thermalization, to optical phonons outside the photoexcitation spot, due to a significant electron diffusion current. Here, we need to estimate the diffusion length of hot electrons within the thermalization time. Considering a diffusion coefficient D for electrons in silicon of 36 $cm^2\,s^{-1}$ and a typical thermalization time of the order of $\tau = 1$ ps [75], we estimate a corresponding diffusion length $L = 2\sqrt{D\tau}$ of about 120 nm. This value is within the same order of magnitude of the Raman measurement spot on the sample and, consequently, we expect that a considerable amount of photoelectrons cannot contribute to optical phonon generation in the Raman measurement region of the sample [see Fig. 6(a)]. In the case of the Si-NCs, a larger amount (nearly all) of the photoexcited electrons contribute to optical phonon excitation in the Raman measurement spot of the sample because of the very small diffusion current associated with the nanoparticulate nature of the system [see Fig. 6(b)] [63]. We should note that this discussion should of course apply also to the photoexcited holes. Typical room-temperature charge transport mobilities μ reported for electrons in Si-NC films are in the range of 10^{-6}–5×10^{-5} $cm^2\,V^{-1}\,s^{-1}$ [76,77]. Using the Einstein relation,

$$D = \frac{k_B T}{e}\mu, \tag{6}$$

these mobility values correspond at maximum to a diffusion coefficient at room temperature of $D = 1.3 \times 10^{-6}$ $cm^2\,s^{-1}$, which gives a negligible diffusion length during thermalization of only ~0.2 Å.

As mentioned above, the spectra of Si-NCs recorded in the optical excitation experiments with high excitation power densities may display more than one peak (see Figs. 1 and 3). The number of peaks and their Ω values do not follow any coherent pattern as a function of excitation power density; however, there is a monotonous correlation between Ω and Γ, which indicates that the origin of the peaks should be the

same, as considered in the analysis above. We note that the appearance of multiple peaks in the Raman spectra should not be due to morphological/structural inhomogeneities of the samples, e.g., inhomogeneous NC size, shape, or surface structure, because such situation would result in a Raman peak broadening instead of multiple peaks. The simplest explanation that we find for the appearance of multiple peaks is the presence, in the same measurement spot, of clusters of Si-NCs experiencing different levels of optical phonon excitation. Si-NC films used in our study are assembled using liquid suspensions composed of agglomerates of Si-NCs with a size typically in range of hundreds of nanometers, which results in the opaque, milky appearance of the suspensions. Therefore, the films form a three-dimensional random network of these Si-NC agglomerates. It is reasonable to assume that different Si-NC agglomerates, with differing shape and number of Si-NCs, may have different electrical conductivities. Taking into account the above discussion, this should in turn result in agglomerates of Si-NCs with different degrees of optical phonon excitation (nonthermal phonon population) within the same measurement spot, consequently yielding multiple peaks in the Raman spectrum. We should also note that for nanoparticulate systems like those used in our study, where electrical percolation effects are very important [77], it is known that the charge transport properties are quite inhomogeneous, where some portions of the system conduct charges more efficiently than others [78]. This explanation is fully consistent with the fact that the multiple peaks appear only at high laser powers because the nonthermal population of phonons occurs only at these excitation powers.

IV. CONCLUSIONS

We monitored the Raman spectra of ensembles of Si-NCs as a function of intensity of optical excitation, with photon energies above the energy band gap (*optical excitation experiments*). We observed that the light intensity dependence of the position Ω of the Raman peak due to the symmetric optical phonon mode in the Si-NCs is significantly steeper than that observed when the same experiments are carried out with bulk *c*-Si. From the measured dependence of Raman spectra on optical excitation intensity, we extracted the corresponding dependence of Ω on temperature T, where T is estimated from the intensity ratio of the Stokes and anti-Stokes Raman peaks. We found that the temperature dependence of Ω observed under the photoexcitation conditions is markedly different from the dependence observed when the same Si-NCs are excited only thermally (*thermal excitation experiments*). For the latter, the Ω versus temperature observed for the Si-NCs corresponds very closely to that observed for bulk *c*-Si. We conclude that moderate/high optical pumping leads to a nonthermal optical phonon population, which is due to an enhanced effect of the electron-phonon coupling resulting from the hindered electrical connectivity in nanoparticulate systems. Under these conditions, the phonon distribution, as well as n and $(p_{n+1})/p_n$, is not only defined by the NCs temperature, but it is also defined by the optical excitation conditions. This phonon nonthermal population affects the position of the Raman band and also leads to an incorrect determination of the temperature using the Stokes/anti-Stokes intensity ratio. Our study indicates that, in nanomaterials with low electrical conductivity and under moderate/high optical excitation intensity, thermometry via Raman spectroscopy becomes unreliable due to a nonthermal population of optical phonons induced by a stronger effect of electron-phonon energy transfer. Under these conditions, the temperature of the system cannot be estimated either from the Raman peak position or from the Stokes/anti-Stokes intensity ratio.

ACKNOWLEDGMENTS

This work has been developed in the scope of the project I3N (Project No. UID/CTM/50025/2013), financed by national funds through the Fundação para a Ciência e a Tecnologia/Ministério da Educação e Ciências (FCT/MEC) and when applicable cofinanced by FEDER under the PT2020 Partnership Agreement. The authors acknowledge also the financial support from Fundação para a Ciência e a Tecnologia (FCT) via Projects No. PTDC/FIS/112885/2009, No. RECI/FIS-NAN/0183/2012(FCOMP-01-0124-FEDER-027494), and No. PTDC/CTM-ENE/2514/2012. This work has been also supported by the Danish Strategic Research Council under the project "Thin-film solar cell based on nanocrystalline silicon and structured backside reflectors (THINC)". R.N.P. acknowledges Martin Stutzmann for stimulating discussion. A.C. acknowledges the Dirección General de Investigación Científica y Técnica via Project No. MAT2015-63955-R.

[1] J. Jehlicka and H. Edwards, Org. Geochem. **39**, 371 (2008).
[2] H. J. Butler, L. Ashton, B. Bird, G. Cinque, K. Curtis, J. Dorney, K. E.-White, N. J. Fullwood, B. Gardner, P. L. M.-Hirsch, M. J. Walsh, M. R. McAinsh, N. Stone, and F. L. Martin, Nat. Protoc. **11**, 664 (2016).
[3] B. Fluegel, A. V. Mialitsin, D. A. Beaton, J. L. Reno, and A. Mascarenhas, Nat. Commun. **6**, 7136 (2015).
[4] G. Xue, Prog. Polym. Sci. **22**, 313 (1997).
[5] J. J. H. Parker, D. W. Feldman, and M. Ashkin, Phys. Rev. **155**, 712 (1967).
[6] J. Menéndez and M. Cardona, Phys. Rev. B **29**, 2051 (1984).
[7] J. J. E. Smith, M. H. Brodsky, B. I. Crowder, and M. I. Nathan, Phys. Rev. Lett. **26**, 642 (1971).
[8] F. Cerdeira, C. J. Buchenauer, F. H. Pollak, and M. Cardona, Phys. Rev. B **5**, 580 (1972).
[9] A. K. Sood, J. Menéndez, M. Cardona, and K. Ploog, Phys. Rev. Lett. **54**, 2111 (1985).
[10] M. R. Correia, S. Pereira, E. Pereira, J. Frandon, I. M. Watson, C. Liu, A. Alves, A. D. Sequeira, and N. Franco, Appl. Phys. Lett. **85**, 2235 (2004).
[11] M. R. Correia, S. Pereira, E. Pereira, J. Frandon, and E. Alves, Appl. Phys. Lett. **83**, 4761 (2003).
[12] V. Y. Davydov, Y. E. Kitaev, I. N. Goncharuk, A. N. Smirnov, J. Graul, O. Semchinova, D. Uffmann, M. B. Smirnov, A. P. Mirgorodsky, and R. A. Evarestov, Phys. Rev. B **58**, 12899 (1998).

[13] G. Kaczmarczyk, A. Kaschner, S. Reich, A. Hoffmann, C. Thomsen, D. J. As, A. P. Lima, D. Schikora, K. Lischka, R. Averbeck, and H. Riechert, Appl. Phys. Lett. **76**, 2122 (2000).

[14] J. Rodrigues, M. Fialho, T. C. Esteves, N. F. Santos, N. B. Sedrine, L. Rino, A. J. Neves, K. Lorenz, E. Alves, and T. Monteiro, J. Appl. Phys. **120**, 081701 (2016).

[15] P. V. Santos, A. K. Sood, M. Cardona, K. Ploog, Y. Ohmori, and H. Okamoto, Phys. Rev. B **37**, 6381 (1988).

[16] S. Piscanec, M. Cantoro, A. C. Ferrari, J. A. Zapien, Y. Lifshitz, S. T. Lee, S. Hofmann, and J. Robertson, Phys. Rev. B **68**, 241312 (2003).

[17] B. P. Falcão, J. P. Leitão, J. C. González, M. R. Correia, K. G. Zayas-Bazán, F. M. Matinaga, M. B. Moreira, C. F. Leite, and A. G. de Oliveira, J. Mater. Sci. **48**, 1794 (2013).

[18] J. Rodrigues, M. F. Leitão, J. F. C. Carreira, N. B. Sedrine, N. F. Santos, M. Felizardo, T. Auzelle, B. Daudin, E. Alves, A. J. Neves, M. R. Correia, F. M. Costa, K. Lorenz, and T. Monteiro, J. Phys. Chem. C **119**, 17954 (2015).

[19] R. Lechner, A. R. Stegner, R. N. Pereira, R. Dietmueller, M. S. Brandt, A. Ebbers, M. Trocha, H. Wiggers, and M. Stutzmann, J. Appl. Phys. **104**, 053701 (2008).

[20] A. V. Kolobov, Y. Maeda, and K. Tanaka, J. Appl. Phys. **88**, 3285 (2000).

[21] A. C. Ferrari, J. C. Meyer, V. Scardaci, C. Casiraghi, M. Lazzeri, F. Mauri, S. Piscanec, D. Jiang, K. S. Novoselov, S. Roth, and A. K. Geim, Phys. Rev. Lett. **97**, 187401 (2006).

[22] L. M. Malard, M. A. Pimenta, G. Dresselhaus, and M. S. Dresselhaus, Phys. Rep. **473**, 51 (2009).

[23] C. Bouhafs, V. Darakchieva, I. L. Persson, A. Tiberj, P. O. Å. Persson, M. Paillet, A.-A. Zahab, P. Landois, S. Juillaguet, S. Schöche, M. Schubert, and R. Yakimova, J. Appl. Phys. **117**, 085701 (2015).

[24] M. S. Dresselhaus, G. Dresselhaus, R. Saito, and A. Jorio, Phys. Rep. **409**, 47 (2005).

[25] D. Mata, R. M. Silva, A. J. S. Fernandes, F. Oliveira, P. M. F. J. Costa, and R. F. Silva, Carbon **50**, 3585 (2012).

[26] J. Rodrigues, D. Mata, A. J. S. Fernandes, M. A. Neto, R. F. Silva, T. Monteiro, and F. M. Costa, Acta Mater. **60**, 5143 (2012).

[27] M. Balkanski, R. F. Wallis, and E. Haro, Phys. Rev. B **28**, 1928 (1983).

[28] H. Brugger and P. W. Epperlein, Appl. Phys. Lett. **56**, 1049 (1990).

[29] T. Beechem, A. Christensen, S. Graham, and D. Green, J. Appl. Phys. **103**, 123501 (2008).

[30] X. Chen and X. Wang, J. Phys. Chem. C **115**, 22207 (2011).

[31] E. Chávez-Ángel, J. S. Reparaz, J. Gomis-Bresco, M. R. Wagner, J. Cuffe, B. Graczykowski, A. Shchepetov, H. Jiang, M. Prunnila, J. Ahopelto, F. Alzina, and C. M. S. Torres, APL Mater. **2**, 012113 (2014).

[32] G. D. Pazionis, H. Tang, and I. P. Herman, IEEE J. Quantum Electron. **25**, 976 (1989).

[33] I. D. Wolf, Semicond. Sci. Technol. **11**, 139 (1996).

[34] A. Link, K. Bitzer, W. Limmer, R. Sauer, C. Kirchner, V. Schwegler, M. Kamp, D. G. Ebling, and K. W. Benz, J. Appl. Phys. **86**, 6256 (1999).

[35] V. I. Belitsky, A. Cantarero, M. Cardona, C. Trallero-Giner, and S. T. Pavlov, J. Phys.: Condens. Matter **9**, 5965 (1997).

[36] A. Compaan, M. C. Lee, and G. J. Trott, Phys. Rev. B **32**, 6731 (1985).

[37] H. Tang and I. P. Herman, Phys. Rev. B **43**, 2299 (1991).

[38] D. M. Sagar, J. M. Atkin, P. K. B. Palomaki, N. R. Neale, J. L. Blackburn, J. C. Johnson, A. J. Nozik, M. B. Raschke, and M. C. Beard, Nano Lett. **15**, 1511 (2015).

[39] H. Richter, Z. Wang, and L. Ley, Solid State Commun. **39**, 625 (1981).

[40] Z. Iqbal and S. Veprek, J. Phys. C: Solid State Phys. **15**, 377 (1982)

[41] I. Campbell and P. Fauchet, Solid State Commun. **58**, 739 (1986).

[42] G. Viera, S. Huet, and L. Boufendi, J. Appl. Phys. **90**, 4175 (2001).

[43] M. J. Konstantinović, S. Bersier, X. Wang, M. Hayne, P. Lievens, R. E. Silverans, and V. V. Moshchalkov, Phys. Rev. B **66**, 161311 (2002).

[44] G. Faraci, S. Gibilisco, P. Russo, A. R. Pennisi, and S. La Rosa, Phys. Rev. B **73**, 033307 (2006).

[45] Y. Duan, J. F. Kong, and W. Z. Shen, J. Raman Spectrosc. **43**, 756 (2012).

[46] A. S. Nikolenko, Semicond. Phys. Quantum Electron. Optoelectron. **16**, 86 (2013).

[47] G. Faraci, S. Gibilisco, and A. R. Pennisi, Phys. Rev. B **80**, 193410 (2009).

[48] S. Gibilisco, G. Faraci, A. R. Pennisi, and A. Irrera, J. Non-Cryst. Solids **356**, 1948 (2010).

[49] L. Han, M. Zeman, and A. H. M. Smets, Nanoscale **7**, 8389 (2015).

[50] H. S. Mavi, S. Prusty, A. K. Shukla, and S. C. Abbi, Thin Solid Films **425**, 90 (2003).

[51] L. Pavesi, L. D. Negro, C. Mazzoleni, G. Franzò, and F. Priolo, Nature (London) **408**, 440 (2000).

[52] K.-Y. Cheng, R. Anthony, U. R. Kortshagen, and R. J. Holmes, Nano Lett. **11**, 1952 (2011).

[53] F. Maier-Flaig, J. Rinck, M. Stephan, T. Bocksrocker, M. Bruns, C. Kübel, A. K. Powell, G. A. Ozin, and U. Lemmer, Nano Lett. **13**, 475 (2013).

[54] S. Tiwari, F. Rana, H. Hanafi, A. Hartstein, E. F. Crabbé, and K. Chan, Appl. Phys. Lett. **68**, 1377 (1996).

[55] M. L. Ostraat, J. W. D. Blauwe, M. L. Green, L. D. Bell, M. L. Brongersma, J. Casperson, R. C. Flagan, and H. A. Atwater, Appl. Phys. Lett. **79**, 433 (2001).

[56] G. Conibeer, M. Green, R. Corkish, Y. Cho, E.-C. Cho, C.-W. Jiang, T. Fangsuwannarak, E. Pink, Y. Huang, T. Puzzer, T. Trupke, B. Richards, A. Shalav, and K. lung Lin, Thin Solid Films **511-512**, 654 (2006).

[57] E.-C. Cho, M. A. Green, G. Conibeer, D. Song, Y.-H. Cho, G. Scardera, S. Huang, S. Park, X. J. Hao, Y. Huang, and L. V. Dao, Adv. Optoelectron. **2007**, 69578 (2007).

[58] E.-C. Cho, S. Park, X. Hao, D. Song, G. Conibeer, S.-C. Park, and M. A. Green, Nanotechnology **19**, 245201 (2008).

[59] G. Faraci, S. Gibilisco, and A. R. Pennisi, Phys. Lett. A **373**, 3779 (2009).

[60] C. M. Hessel, J. Wei, D. Reid, H. Fuji, M. C. Downer, and B. A. Korgel, J. Phys. Chem. Lett. **3**, 1089 (2012).

[61] A. S. Nikolenko, Ukr. J. Phys. **58**, 980 (2013).

[62] S. Niesar, R. N. Pereira, A. R. Stegner, N. Erhard, M. Hoeb, A. Baumer, H. Wiggers, M. S. Brandt, and M. Stutzmann, Adv. Funct. Mater. **22**, 1190 (2012).

[63] R. N. Pereira, S. Niesar, W. B. You, A. F. da Cunha, N. Erhard, A. R. Stegner, H. Wiggers, M.-G. Willinger, M. Stutzmann, and M. S. Brandt, J. Phys. Chem. C **115**, 20120 (2011).

[64] See Supplemental Material at http://link.aps.org/supplemental/10.1103/PhysRevB.95.115439 for XRD and SEM data supporting the structural characterization of the samples and a description of the experimental determination of the coefficient *F*.
[65] T. Kamei, P. Stradins, and A. Matsuda, Appl. Phys. Lett. **74**, 1707 (1999).
[66] G. Faraci, A. R. Pennisi, A. Alberti, R. Ruggeri, and G. Mannino, Sci. Rep. **3**, 2674 (2013).
[67] T. Okada and K. Yamamoto, Jpn. J. Appl. Phys. **26**, 2134 (1987).
[68] V. Poborchii, T. Tada, and T. Kanayama, J. Appl. Phys. **97**, 104323 (2005).
[69] Y. Okada and Y. Tokumaru, J. Appl. Phys. **56**, 314 (1984).
[70] C. Postmus, J. R. Ferraro, and S. S. Mitra, Phys. Rev. **174**, 983 (1968).
[71] G. E. Jellison, D. H. Lowndes, and R. F. Wood, Phys. Rev. B **28**, 3272 (1983).
[72] L. Khriachtchev, M. Räsänen, and S. Novikov, J. Appl. Phys. **100**, 053502 (2006).
[73] H. Koyama and P. M. Fauchet, J. Appl. Phys. **87**, 1788 (2000).
[74] W.-L. Ong, S. M. Rupich, D. V. Talapin, A. J. H. McGaughey, and J. A. Malen, Nat. Mater. **12**, 410 (2013).
[75] F. E. Doany and D. Grischkowsky, Appl. Phys. Lett. **52**, 36 (1988).
[76] R. N. Pereira, J. Coutinho, S. Niesar, T. A. Oliveira, W. Aigner, H. Wiggers, M. J. Rayson, P. R. Briddon, M. S. Brandt, and M. Stutzmann, Nano Lett. **14**, 3817 (2014).
[77] W. Aigner, M. Wiesinger, H. Wiggers, M. Stutzmann, and R. N. Pereira, Phys. Rev. Appl. **5**, 054017 (2016).
[78] B. Stoib, T. Langmann, S. Matich, T. Antesberger, N. Stein, S. Angst, N. Petermann, R. Schmechel, G. Schierning, D. E. Wolf, H. Wiggers, M. Stutzmann, and M. S. Brandt, Appl. Phys. Lett. **100**, 231907 (2012).